ELSEVIER

Journal of Nuclear Materials 266–269 (1999) 581–586

journal of nuclear materials

Erosion of beryllium and deposition of carbon and oxygen due to bombardment with C^+ and CO^+ ions

P. Goldstraß, W. Eckstein, Ch. Linsmeier *

Max-Planck-Institut für Plasmaphysik, EURATOM-Association, Boltzmannstr. 2, D-85748 Garching, Germany

Abstract

The bombardment of clean, metallic beryllium with carbon and the co-bombardment with carbon and oxygen is investigated experimentally and by computer simulation. The experiments use C^+ and CO^+ ions with energies between 3 and 12 keV at normal incidence. The simulation is carried out with the Monte Carlo code TRIDYN. The results of carbon bombardment from experiment and simulation agree well and show the buildup of a carbon adlayer on the metal surface. After the carbon adlayer formation, no more Be is eroded. For C and O co-bombardment, carried out by CO^+ ion bombardment, simulation and experiment agree for low fluences. At higher fluences, another erosion channel besides kinematic sputtering is opened by the chemical interactions of C and O. This leads to a deposition/erosion equilibrium which is not predicted by the kinematic TRIDYN code. The formation of a ternary mixture layer on the Be target leads to a continuous erosion of the beryllium target.

Keywords: Beryllium; Erosion; Deposition; Carbon ions

1. Introduction

In the design of future fusion plasma devices like ITER several elements are regarded as possible first wall materials. Both, low-Z elements as Be and C, and heavy elements as Mo and W are under discussion. If these elements are eroded from walls or divertor plates, they will eventually lead to impurity contamination of the discharge. In this case plasma facing components will be bombarded simultaneously with hydrogen isotopes and these impurity species. Of the low-Z elements Be has been used in JET [1] and C in most fusion machines. Earlier investigations have shown that experimental data are well reproduced by simulations for the bombardment of W with C only [2]. Some information on Be is given in [3,4]. Therefore, in this paper the effects of a simultaneous bombardment of Be with C and O from CO^+ are investigated experimentally and compared to computer simulations to validate the modelling of this more complex situation.

2. Experiment

A polycrystalline polished Be target was bombarded at normal incidence with 3 and 5 keV C^+ and 3, 5 and 12 keV CO^+ ions in the apparatus BOMBARDON [5]. The ions are produced by an electron impact source from CO gas (Linde 3.7) and subsequently mass-separated by a 80° magnetic deflection. The base pressure in the target chamber and during the RBS analysis was in the low 10^{-11} hPa range, during the implantation in the 5×10^{-11} hPa range. The Be target was cleaned by periodic 5 keV Ar^+ bombardment and annealing to 680 K. Analysis of the implanted C and O was performed by Rutherford backscattering spectroscopy (RBS) using 0.6 MeV $^4He^+$ at normal incidence. The detector was situated at a scattering angle of 163°. Implantation and subsequent RBS analysis were all carried out with the sample at room temperature.

Fig. 1 shows RBS spectra of the sample after cleaning (a) and after CO^+ implantation (b). The spectrum (a) of the clean sample exhibits the Be edge and peaks originating from Ar caused by the cleaning procedure, as well as a small signal from tantalum. The Ta surface contamination is caused by sputter deposition of Ta

* Corresponding author. Tel.: +49 89 3299 1263; fax: +49 89 3299 1149 e-mail: linsmeier@ipp.mpg.de

0022-3115/99/$ – see front matter
PII: S0022-3115(98)00545-5

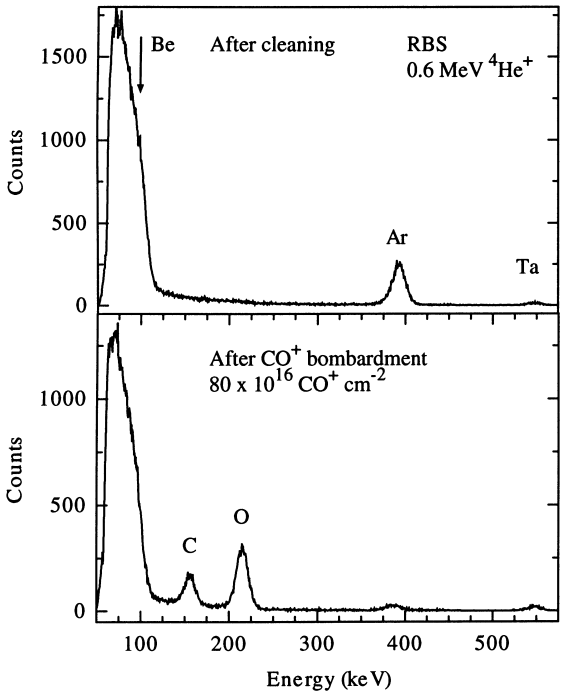

Fig. 1. Energy distributions of backscattered ^4He from a clean Be target (a) and a Be target bombarded with 5 keV CO^+ ions (b). The CO^+ fluence is 8.0×10^{17} cm^{-2}. Analysis is performed with 0.6 MeV $^4He^+$, the backscattering angle is 163°.

from an aperture used in early steps of the cleaning procedure. The Ta intensity corresponds to an amount of 6.0×10^{13} cm^{-2} (about 0.04 monolayers). No carbon and oxygen can be detected after the cleaning procedure. Spectrum (b) in Fig. 1 shows the RBS analysis of the Be target after bombardment with 8×10^{17} CO^+ cm^{-2} at 5 keV. It demonstrates well the separation of the C and O peaks and the Be edge. Due to the CO^+ bombardment, the Ar amount has decreased by a factor of about 26. The C and O amounts in the sample are determined by integration of the respective peak areas after background subtraction. The peak widths of both the C and O signals are comparable to the submonolayer signal from the Ta peak, which give an energy resolution of the detection system of 18.7 keV. The corresponding depth resolution of 650 Å (calculated for the stopping in Be metal) is not good enough to extract depth profiles from the measured spectra.

3. Simulation

The calculations were performed with the Monte Carlo program TRIDYN (version 40.3) [6,7]. This program takes into account all collisional effects as implantation, reflection, and sputtering. Target composition changes due to the bombardment are regarded as well, so that effects like sputter yields, reflection coefficients, and composition profiles can be determined as a function of the bombarding fluence. The program allows also simultaneous bombardment with several species of fixed energy or with a Maxwellian incident distribution. Surface binding energies, important for sputtering, are based on the elemental heats of sublimation and are interpolated due to the surface composition of the target [8]. Chemical erosion, diffusion and segregation are neglected. The sample is divided in thin layers of 2.5 Å thickness which may have different compositions. The output step is usually 1% of the total fluence applied. The composition of each layer is adjusted after processing every collision cascade. Thus, compositional changes due to the incoming ions are taken into account.

4. Results and discussion

4.1. C^+ implantation

The Be target was bombarded after cleaning with C^+ ions up to a fluence of 5.5×10^{17} cm^{-2}. The maximum fluence was determined by the lifetime of the ion source filament. Fig. 2 shows the calculated depth distribution of 5 keV C^+ implanted in beryllium for several fluences which correspond to the experimentally applied values. Beginning with 5×10^{16} cm^{-2}, carbon is deposited in a depth of roughly 200 Å with almost no carbon at the sample surface. For higher fluences, the carbon con-

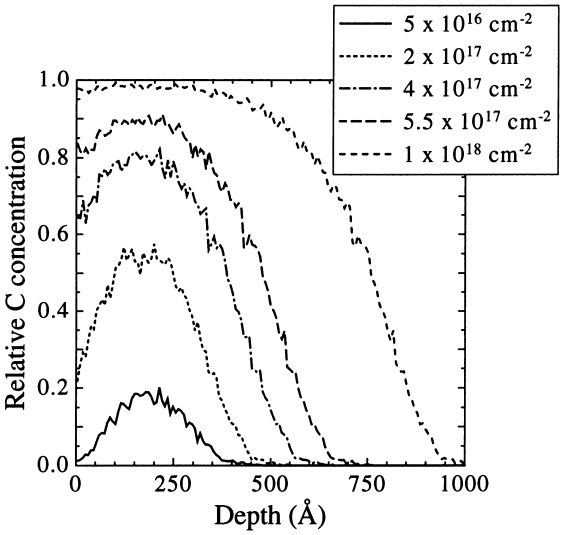

Fig. 2. Depth distributions of C in Be. Be is bombarded with 5 keV C^+ at normal incidence (TRIDYN). The calculated fluences correspond to the values of the experiments.

centration on the target surface increases up to almost unity and the buildup of a carbon layer with increasing thickness is expected. The further steps resulting in this adlayer formation are the erosion of the beryllium on the target surface above the implantation zone. During extended C^+ bombardment, the deposition zone with implanted carbon is finally reached. Since the self sputtering yield of C^+ on pure carbon is below unity [3], carbon then builds up a layer on the Be substrate. Under further C^+ ion bombardment, this carbon surface layer grows steadily.

The experimental results confirm the predictions from the TRIDYN simulation. Fig. 3 shows the deposited amount of carbon on the target as a function of the C^+ fluence. The lines represent the TRIDYN calculations for a primary energy of the C^+ ions of 3 and 5 keV. The data points are the measured carbon concentrations in the Be target after the C^+ bombardment. Each experiment consists of one or more series, each starting with a clean Be surface containing no carbon and oxygen (cleanliness corresponding to spectrum of Fig. 1(a)). The lines represent simulations with KrC [9] and ZBL [10] interaction potentials. The difference between them is negligible and not visible in the diagram. The amount of deposited carbon after ion bombardment is calculated from the carbon peak area in the RBS spectra after background subtraction. For 5 keV C^+ the agreement between simulation and experiment is excellent. For 3 keV a deviation between the Monte Carlo

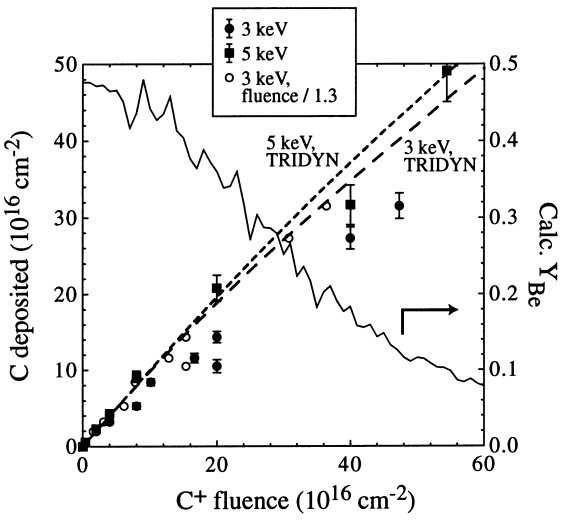

Fig. 3. Deposited C on the Be target versus the C^+ fluence due to the bombardment with 3 and 5 keV C^+ at normal incidence. The TRIDYN calculations are performed with the KrC and ZBL interaction potentials. The difference between the two interaction potentials is negligible and not shown in the diagram. Also shown is the calculated sputtering yield of Be considering the compositional changes due to the C^+ bombardment.

calculation and the data points from RBS analysis can be recognized. However, the shape of the calculated line fits very well to the data points if these are scaled by a factor of 1.3. The scaling can be done either on the C^+ fluence or on the intensity axis to achieve this agreement. Since the deposited fluence is determined experimentally by integrating the current collected on the target and the surrounding Faraday cup during implantation, an error in the current measurement leads to an error in the C^+ fluence determination. Therefore, the agreement between the TRIDYN simulation and the RBS measurement can be regarded as satisfiable for both primary energies. The error bars at the experimental data points in Fig. 3 account only for the statistical error in the RBS spectra and do not reflect uncertainties in the current measurement.

As predicted by the simulation, the experiments show the buildup of a carbon layer on the sample surface. In the studied fluence range no saturation in the deposited amount of carbon is found. The carbon layer thickness at the maximum experimental C^+ fluence of 5.48×10^{17} cm^{-2} is 483 Å, calculated for a graphite density of 2.26 g cm^{-3}. This is in good agreement with the result from the calculation (Fig. 2), where the carbon concentration starts to decrease at a depth of about 500 Å. However, the maximum carbon concentration in the calculation is only 98%, but the additional carbon in deeper layers leads to a total amount of carbon comparable to that detected in the RBS experiments. The carbon layer at the maximum fluence after 3 keV C^+ bombardment (4.73×10^{17} cm^{-2}) reaches a thickness of 417 Å.

Both experiment and TRIDYN simulation in Fig. 3 show a change in the slope of the C amount with increasing fluence. This can be attributed to a compositional change in the surface layer during C^+ implantation. The carbon peak deposition zone is in a depth of approximately 200 Å. The sputtering process due to the collision cascades takes place at the outermost layers. This leads to an erosion of the mixed Be–C layer at the surface above the C implantation zone. This process continues until the surface layer consists predominantly of carbon. The gradual change in the composition results in an increase of the C^+ reflection. However, the reflected fraction of primary ions stays well below 0.2% for both primary energies. For high C concentrations after greater fluences, the erosion of the Be–C mixed layer decreases and the C adlayer formation continues. This leads finally to a surface layer consisting almost exclusively of carbon, and as a consequence to the continuous build-up of a carbon layer on the beryllium substrate.

4.2. CO^+ implantation

Since the CO^+ currents from the ion source are much larger than for C^+, implantation fluences up to

2×10^{18} cm^{-2} are accessible in the experiment. Compared to the C^+ beams, the carbon and oxygen atoms impinging on the surface from CO^+ beams have lower energies. The kinetic energy is split between the atoms in the CO^+ molecule according to their mass ratio of C (3/7) and O (4/7). Therefore, carbon possesses energies around 1.286, 2.143 and 5.145 keV for the 3, 5 and 12 keV primary beams, whereas oxygen has energies of 1.714, 2.857 and 6.855 keV, respectively.

At low fluences below approximately 1×10^{17} cm^{-2}, the experimentally measured amounts of deposited carbon and oxygen in the sample increase according to the calculations by the TRIDYN program, see Fig. 4. This behaviour is similar to that of the C^+ bombardment and can be explained by the implantation of both C and O in the Be matrix. The ion bombardment also leads to a simultaneous sputtering of beryllium. Both carbon and oxygen are deposited in an implantation zone below the surface. The depth and width of this zone depend on the primary energy of the CO^+ ions. Fig. 5 shows TRIM.SP results for CO^+ ions, impinging on Be at three different energies, respectively. In contrast to TRIDYN, TRIM.SP does not account for compositional changes in the target due to ion bombardment. Since the kinetic energy splits asymmetrically between C and O upon CO^+ impact on the surface and these two species exhibit different stopping cross-sections on their path through the target, their depth distribution depends on the CO^+ primary energy. For 3 keV CO^+, the peak implantation zone is around a depth of 60 Å. Oxygen is implanted slightly deeper than carbon. For 5 keV CO^+, the implantation maximum is around a depth of 80 Å. Again, oxygen is deposited slightly deeper than carbon. The difference in implantation depth between C and O vanishes for a primary CO^+ ion energy of 12 keV and the maximum of the deposition zone lies around 200 Å. It can also be noted that the width of the implantation zones increases strongly with increasing CO^+ primary energy. The calculation pictured in Fig. 5 reflects the very beginning of the CO^+ implantation and corresponds to zero fluence, since no compositional changes due to the ion beam are taken into account by TRIM.SP. For continued CO^+ bombardment, the beryllium above the C and O deposition zones is eroded by sputtering. The actual sample surface recesses and subsequent C and O are deposited accordingly in greater depths. This will lead eventually to the formation of a mixed layer consisting of the three elements C, O and Be which starts at the surface and extends into the sample. In contrast to the C^+ implantation scenario, the ternary system of C, O and Be is expected to show a more complex behaviour, which is demonstrated in the experimental results.

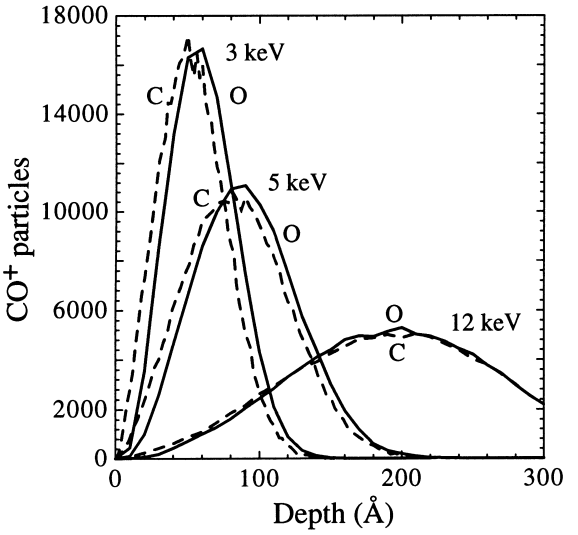

Fig. 5. Implantation zones for carbon and oxygen at 3, 5 and 12 keV, resulting from the asymmetric splitting of the kinetic energy of the CO^+ ion upon target impact and subsequent stopping in beryllium. Calculations are carried out by TRIM.SP and represent the zero fluence case (no compositional changes in the target due to the ion beam are considered).

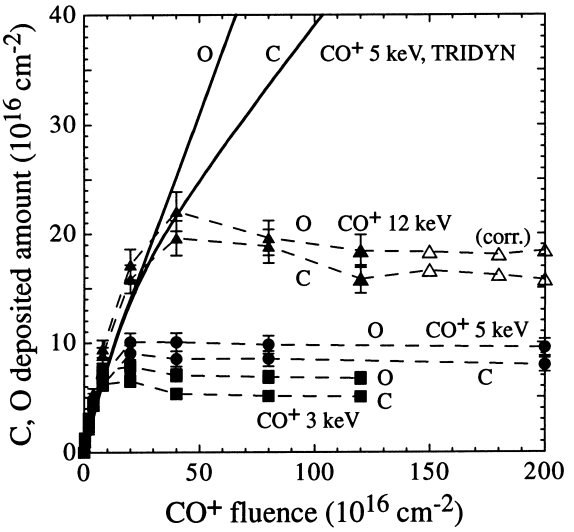

Fig. 4. Deposited C and O in the Be target versus the fluence due to the bombardment with 3, 5 and 12 keV CO^+ at normal incidence. Lines between the experimental data points are drawn to guide the eye. (The 12 keV CO^+ data points at fluences $>1.3\times10^{18}$ cm^{-2} (open symbols) are corrected due to an error in the current measurement.)

The C and O concentrations start to saturate at a fluence which depends on the CO^+ primary energy. Fig. 4 shows a deviation of the RBS results from the TRIDYN calculations at fluences between 4×10^{16} cm^{-2} and 3×10^{17} cm^{-2}, depending on the CO^+ energies. Only shown is the TRIDYN calculation for 5 keV CO^+ ions, since the difference for 3 and 12 keV in the valid fluence regime below approx. 1.5×10^{17} cm^{-2} is negligible. The C

and O concentrations start to saturate and reach an energy-dependent, constant value. The measurements also suggest that the amounts of deposited C and O pass through a maximum before reaching their saturation value. This saturation effect cannot be explained by mere atomic collisions and is therefore not predicted by the TRIDYN calculations. The experiments demonstrate that after a certain transition fluence an erosion mechanism other than collisional sputtering sets in. It leads to a constant C/O ratio and to a constant C and O inventory in the ternary compound formed on the beryllium target. This erosion mechanism releases C and O in equal amounts and is presumably of chemical nature. In experiments dealing with carbon erosion by oxygen, an erosion yield of about unity is found [3,11,12]. The formation of CO and CO_2 by chemical erosion of graphite and beryllium was observed under O^+ irradiation [13,14]. As observed in the O^+ ion experiments [14] this process may also be effective here only after an appreciable C concentration has been accumulated on the surface and after this layer is saturated in oxygen.

The reason for the initial increase in deposited carbon and oxygen, as predicted by the kinematic simulations, is the implantation of C and O in deeper layers. For the erosion mechanism via the formation of CO molecules and their subsequent desorption, a sufficiently high density of both C and O in the Be matrix is necessary. Moreover, the loss of CO by desorption is only possible at the outermost surface. Therefore, two criteria have to be fulfilled before CO erosion can take place and the observed deposition/erosion equilibrium sets in: (1) accumulation of C and O in a sufficiently high density for the formation of the CO molecules. This implies also that the substrate temperature (always room temperature in these experiments) may play an important role, since elevated temperatures will increase the mobility of implanted C and O species. Criterion (2) is the possibility for formed CO to desorb. This can only take place for CO reaching the target surface, either by the formation of CO molecules at the very surface or by diffusion of CO molecules from their formation location to the outermost surface. The increasing onset fluence, the increasing overall C and O inventories and the observed increasing C/O ratios for increasing CO^+ ion energies support this interpretation, as will be discussed in the following paragraphs.

The onset fluence for CO desorption reflects the depth of the implantation zone for C and O. For greater CO^+ primary energies this depth is larger and therefore a greater fluence is necessary to erode the overlying Be layer. Only after the implantation zone is sputtered, C- and O-containing material reaches the surface (CO formation at the surface) or the CO diffusion path length is long enough for CO to reach the surface (CO formation in deeper layers).

The increasing overall C and O inventory for increasing CO^+ primary energies is a consequence of the broader depth distribution for CO^+ ions with higher energies, see Fig. 5. This broader distribution leads to a greater thickness of the C–O–Be ternary mixture layer on the Be target and consequently to a greater C and O equilibrium concentration. Experimentally, the thickness of the ternary adlayer on the Be substrate is reflected in the shift of the Be edge in the RBS spectra. However, the edge shift compared to the edge of the clean Be sample is at the limit of the experimental resolution and may only be taken as a supportive argument.

The different C/O equilibrium ratios for the examined primary energies result from the difference in ion ranges and stopping cross-sections for C^+ and O^+ at their respective energies. For low primary energies, oxygen is implanted at slightly greater depths than carbon. After extended bombardment (after erosion of the Be layer above the implantation zone), the oxygen zone extends further into the sample than the carbon zone. This difference vanishes with increasing CO^+ primary energy, as shown in Fig. 5 by the TRIM.SP simulation. The different thicknesses of the C- and O-containing layers at equilibrium lead to the different average C/O ratios of 0.75, 0.85 and 0.90 for the three respective CO^+ primary energies of 3, 5 and 12 keV. For higher ion energies, the C/O ratio approaches 1, since the implantation depths of C and O become equal.

The consequence of the equilibrium concentrations in the case of a C and O co-bombardment is an equilibrium composition of a ternary adlayer of finite thickness. This implies a continuous erosion of Be in addition to the CO desorption. Therefore, the chemical CO formation process, accompanied by kinematic sputtering, results in a continuous Be target erosion. The different steps in the CO^+ interaction with the beryllium target are summarized in Fig. 6. Step 1 depicts the low fluence regime, where incoming CO^+ are implanted in the Be matrix. CO^+ also leads to sputtering of Be at the surface. This leads to an erosion of the original sample surface. The full separation of the C- and O-containing zones in this picture is for clarification of the process only. For continued CO^+ bombardment (step 2 in Fig. 6), the implantation zone is extended into the Be sample, since the surface is continually eroded. The carbon- and oxygen-containing implantation zones start to overlap in this model. In reality, however, both implantation layers will be overlapping already from the beginning, as is shown in Fig. 5 according to the TRIM.SP calculations. As long as there is a Be layer above the implantation zones, all incoming CO^+ are trapped (except the very small amount of reflected particles, well below 0.2% according to the calculations). This regime corresponds to the low fluences in Fig. 4, which is well reproduced by the TRIDYN simulations. When the implantation zones reach the sample surface (step 3 in Fig. 6), the emission of CO starts and deposition and erosion equilibrate.

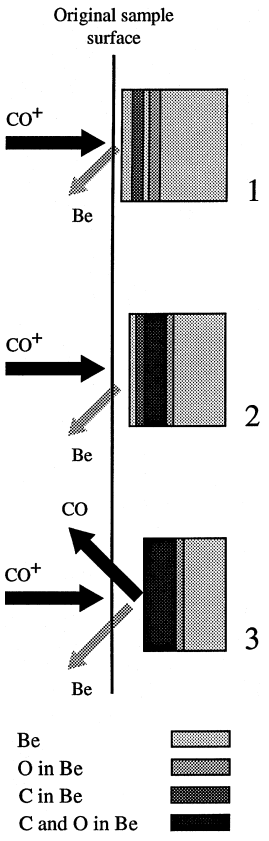

Fig. 6. Schematic description of the CO^+ ion-target interaction. Step 1: Implantation of C and O in different depths, according to their respective energies and stopping cross-sections. Step 2: Continued erosion of Be above the implantation regimes, extended implantation in deeper layers. Step 3: Start of CO erosion, continued Be erosion. Deposition/erosion equilibrium sets in.

This regime finally leads to the constant ternary layer composition, which is found in the experiments.

5. Conclusions

It is shown that the experimental data are in good agreement with results calculated by the kinematic Monte Carlo code TRIDYN for 3 and 5 keV C^+ ions bombarding a clean beryllium target under perpendicular incidence. The interaction of the incoming ions with the target is fully explained by kinematic processes like implantation, reflection and sputtering. A carbon layer of increasing thickness is formed on top of the beryllium metal. After a fluence of approximately 1×10^{18} cm^{-2} no more Be is eroded.

Co-bombardment of beryllium with carbon and oxygen, simulated by the implantation of CO^+ ions in Be, shows a different behaviour. For low fluences, depending on the CO^+ primary energy, a kinematic description of the ion-target interaction is sufficient. TRIDYN simulation and experiment both agree in the accumulation of carbon and oxygen in the Be target. However, after an energy-dependent fluence, another – presumably chemical – erosion mechanism dominates the ion-target interaction. This leads to a constant composition in the target surface layers. Both the composition and the thickness of the formed layer depend on the energy of the incoming CO^+ ions. The absolute amounts of C and O reach constant values for extended CO^+ implantation which means that the Be target surface is continuously eroded. The underlying chemical processes for this behaviour, which may imply the formation of BeO, Be_2C and additional compounds in the ternary layer, and the formation and transport of CO molecules as the desorbing species in the erosion process, are not yet identified and subject to further studies.

Acknowledgements

The authors thank R. Bastasz for the polished Be target.

References

[1] The JET team: presented by P.R. Thomas, J. Nucl. Mater. 176&177 (1990) 3.
[2] W. Eckstein, J. Roth, Nucl. Instr. and Meth. B 53 (1991) 279.
[3] W. Eckstein, C. Garcá-Rosales, J. Roth, W. Ottenberger, IPP-Report 9/82, Garching, 1993.
[4] J. Roth, W. Eckstein, M. Guseva, Fus. Engi. Design 37 (1997) 465.
[5] M. Mayer, W. Eckstein, B.M.U. Scherzer, J. Appl. Phys. 77 (1995) 6609.
[6] W. Eckstein, Computer Simulation of Ion–Solid Interaction, Springer, Berlin, 1991.
[7] W. Möller, W. Eckstein, J.P. Biersack, Comput. Phys. Commun. 51 (1988) 355.
[8] W. Eckstein, M. Hou, V.I. Shulga, Nucl. Instr. and Meth. B 119 (1996) 477.
[9] W.D. Wilson, L.G. Haggmark, J.P. Biersack, Phys. Rev. B 15 (1977) 2458.
[10] J.F. Ziegler, J.P. Biersack, U. Littmark, in: J.F. Ziegler (Ed.), The Stopping and Range of Ions in Matter, vol. 1, Pergamon, New York, 1985.
[11] J. Roth, J. Nucl. Mater. 145–147 (1987) 87.
[12] V. Vietzke, T. Tanabe, V. Philipps, M. Erdweg, K. Flaskamp, J. Nucl. Mater. 145–147 (1987) 425.
[13] V. Vietzke, A. Refke, V. Philipps, M. Hennes, J. Nucl. Mater. 220–222 (1995) 249.
[14] A. Refke, V. Philipps, E. Vietzke, M. Erdweg, J. von Seggern, J. Nucl. Mater. 212–215 (1994) 1255.